Materials Today • Volume xxx, Number xx • xxxx 2019 RESEARCH

ELSEVIER

RESEARCH: Review

Spectral converters for photovoltaics – What's ahead

Rute A.S. Ferreira [1,*], Sandra F.H. Correia [1], Angelo Monguzzi [3], Xiaogang Liu [2], Francesco Meinardi [3,*]

[1] Department of Physics and CICECO – Aveiro Institute of Materials, University of Aveiro, Portugal
[2] Department of Chemistry, National University of Singapore, Singapore
[3] Dipartimento di Scienza dei Materiali, Università degli Studi di Milano-Bicocca, Italy

The effective incorporation of photovoltaic (PV) elements into the urban environment, specifically in buildings, is a challenging process. Apart from the aesthetic limitations of having black and opaque PV cells when installed in building façades, they are not optimally positioned for high-efficiency electric energy generation because of shadowing effects due to neighboring trees and buildings. Emphasis is given to luminescent solar concentrators (LSCs) that have emerged as an appealing solution for concentrating a large area of sunlight into a small beam of high field intensity. The coupling of PV cells to the edges of LSCs also presents an exciting strategy to PV urban integration. Here, we outline the mechanistic framework for LSCs, review the current experimental state of the art involving optically active centers in various geometrical device configurations, and discuss the performance quantification of LSCs currently in development. For the sake of completeness, a brief discussion of the other spectral converters suitable for PV applications is also reported.

Introduction

According to the United Nations (UN) 2030 Agenda for Sustainable Development, the main objectives for the next fifteen years include taking urgent action on climate change and boosting the planetary protection from degradation through sustainable management of its natural resources, production and consumption [1]. To this end, the use of clean and affordable energies is a crucial challenge. In line with the UN, the European Union promotes the construction of zero-energy buildings that can produce more energy than they consume [2–4].

Solar energy is one of the primary renewable energy sources [5], and the advances in photovoltaic (PV) technology allow us to convert solar radiation into electricity. The most efficient (larger power conversion efficiency, PCE) single-junction PV cells are based on GaAs (PCE values ~29%), single-crystalline Si (c-Si, PCE values ~27%) and copper indium gallium selenide (CIGS, with PCE values up to ~23%). Depending on the specific application, the most common commercial PV cells are based on single-crystalline Si (c-Si) and, although presenting lower efficiencies, on multicrystalline-Si (mc-Si) and amorphous Si (a-Si), with PCE values of ~22% and ~10%, respectively [6]. Organic and dye-sensitized solar cells (DSSCs) have been deeply investigated in the last two decades but their overall performances are still far from those of the inorganic PVs, thus actually resulting competitive only for very specific applications as in low-light indoor conditions [7,8]. Also, it is worth mentioning that perovskite-based PV cells, over the last few years, have gained visibility due to the unprecedented increase in their PCE values in such a short time [9]. Common to all, the mismatch between the solar spectral irradiance (AM1.5G spectrum) and the absorption maxima limits their efficiency, particularly the utility for large-land deployment (Fig. 1a). Focusing our attention into the Si-based PV cells as they represent about 95% of the market [10], photon management can be used to increase the photon absorption ability, Fig. 1b. In the case of downconversion (DC, or quantum-cutting), an incident high energy photon is converted

* Corresponding authors.
E-mail addresses: Ferreira, R.A.S. (rferreira@ua.pt), Meinardi, F. (francesco.meinardi@unimib.it).

 https://doi.org/10.1016/j.mattod.2019.10.002

Please cite this article in press as: R.A.S. Ferreira et al., Materials Today, (2019), https://doi.org/10.1016/j.mattod.2019.10.002

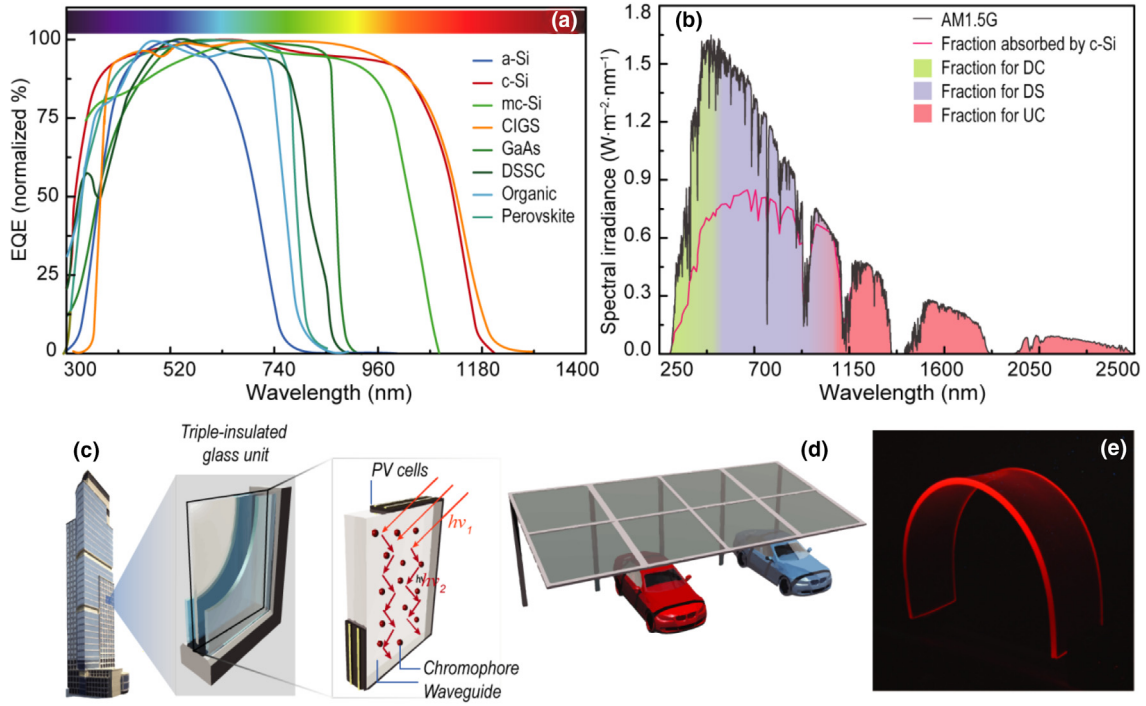

FIGURE 1

Spectral converters for PV devices and AM1.5G spectrum. (a) Normalized external quantum efficiency for single-junction PV cells with confirmed terrestrial efficiencies measured under the global AM1.5 spectrum (1000 W·m^{-2}) at a cell temperature of 25 °C, according to [6]. (b) AM1.5G solar spectral irradiance spectrum. The shadowed areas represent the fraction available for DC (26%, up to 550 nm), DS (81%, up to 1100 nm) and UC (16%, in the 1200–2500 nm range) for a c-Si wafer. The fraction absorbed by c-Si is also indicated [23]. Schematic representation of urban integration of LSCs such as (c) PV window consisting of a triple-insulated glass unit embedding a LSC replacing the inner glass panel (h, Planck's constant; ν, frequency) and (d) as parking coverages. (e) Photograph of a flexible LSC composed of Si nanocrystals under UV illumination (adapted with permission from Springer Nature DOI: https://doi.org/10.1038/natrevmats.2017.72 [17]).

into two photons with lower energy, which can lead to an emission quantum yield (QY) up to QY $\leq$ 200%; in upconversion (UC), two low energy photons are converted into one high energy photon, QY $\leq$ 50%; down-shifting (DS) is similar to DC but in this case only one photon is emitted, QY $\leq$ 100%. Spectral converters, such as down-shifting or conversion/upconverting layers [11–16] and luminescent solar concentrators (LSCs) [8,15–22] have been investigated over the past few years.

In general, spectral converters exploit the photoluminescence processes to capture low- or high-energy photons that cannot be used by the PV cell and convert them to photons with a useful energy. The spectral converter layers are additive devices to enhance PV performance, while LSCs are a cost-effective technology [19] to be used in the built environment as they could be embedded in façades or windows (Fig. 1c and d), allowing them to be transformed into energy harvesting units [17]. In this scope, the design options for standard PV cells are limited because PV panels are typically black and non-transparent, which is one of the major problems facing building-integrated PVs [24]. From an aesthetic point of view, LSCs may be an appealing solution since they can be produced in almost any color and shape (Fig. 1e) [25]. There is also the possibility to fabricate fiber-based LSCs, which present some advantages: lightweight, flexibility and the easy coupling to other optical fibers for waveguide amplification and remote light harvesting [26–30].

Another barrier for the implementation of PV panels into the built environment is the fact that PV panels operate optimally only under uniform and direct irradiation, which is not the case for the built environment where sunlight is often diffuse and shaded [31]. LSCs and converting layers operate similarly under direct and diffuse sunlight conditions [32] and can be applied over large areas and easily incorporated into construction elements [33].

Practical examples of LSCs include their utility in highway sound barriers [33–35], an important demonstration towards the transference from laboratory prototypes to real-life solar-energy harvesting units (Fig. 2a). The commercialization of LSCs has reinforced their status quo: (i) the *Glass to Power* company, an Italian spin-off of the University of Milan Bicocca (Fig. 2b) [36], and (ii) *UbiQD* which produces luminescent greenhouses that mimic the late summer Sun (Fig. 2c and d) and solar windows (Fig. 2e) [37]. The ability to fabricate LSCs in thin-film form with tunable emission color provides an extra advantage to enable selective filtering of the Sun, so that the light inside greenhouses is selected towards the control of plant or animal circadian rhythms [38], favoring the growth process and maximizing crop production [39].

Working mechanisms

Spectral conversion down-shifting/down-converter layers (DSL/DCL) are coatings applied on the PV cell top surface (Fig. 3a) able

Please cite this article in press as: R.A.S. Ferreira et al., Materials Today, (2019), https://doi.org/10.1016/j.mattod.2019.10.002

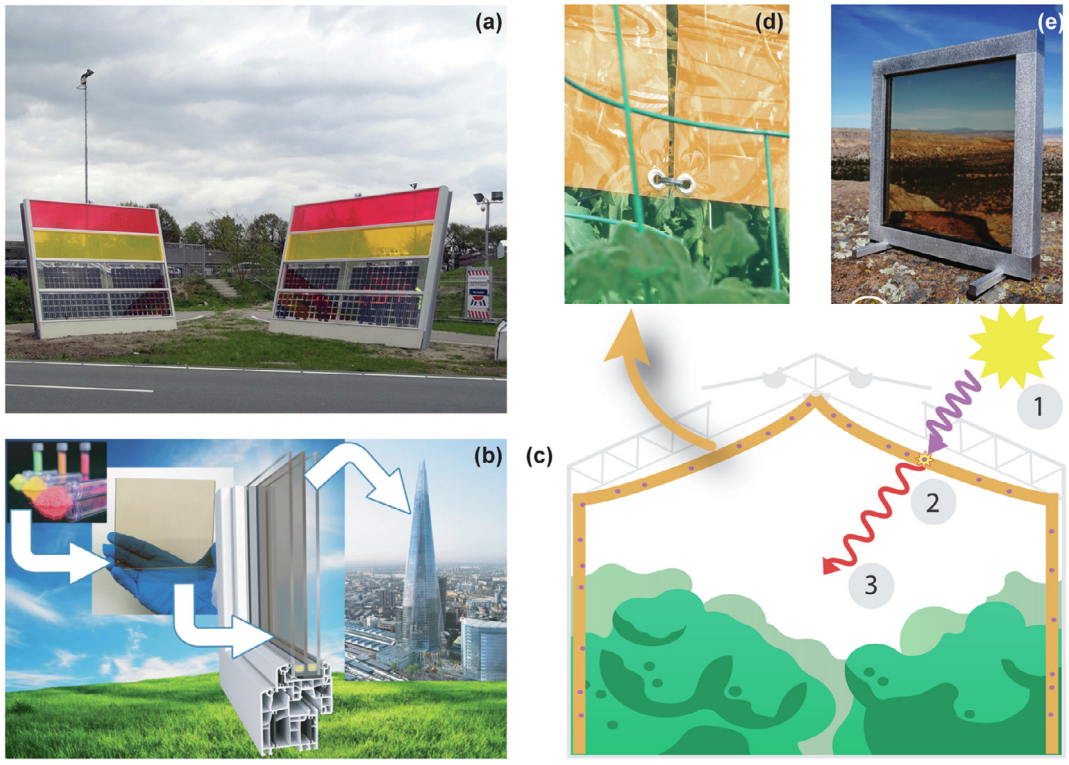

FIGURE 2

Practical examples of luminescent solar concentrators and spectral converter films. (a) Photographs of the LSC-based noise barrier site on the left faces North/South, and the barrier on the right faces East/ West, adapted from DOI: https://doi.org/10.1016/j.renene.2016.10.078, CC BY license (http://creativecommons.org/licenses/by/4.0/). (b) Glass to Power company LSC concept and (c) UbiQD greenhouse scheme with (d) photograph of the UbiGro films. (e) LSC window prototype realized by UbiQD which also employed spectral converters for greenhouse coverages (Courtesy of UbiQD, Inc). Adapted from [33,36,39].

to absorb the incident radiation complementarily to the PV cell, which is re-emitted at a specific wavelength and then refracted towards the PV cell. The use of DSLs allows the tuning of the PV cell absorption spectral range [23]. The DS materials absorb the UV and visible radiation, typically in the 300–500 nm range, and re-emit it at a longer wavelength where the external quantum efficiency (EQE) of the PV device is higher. The lower energy photons emitted by the luminophores upon absorption are

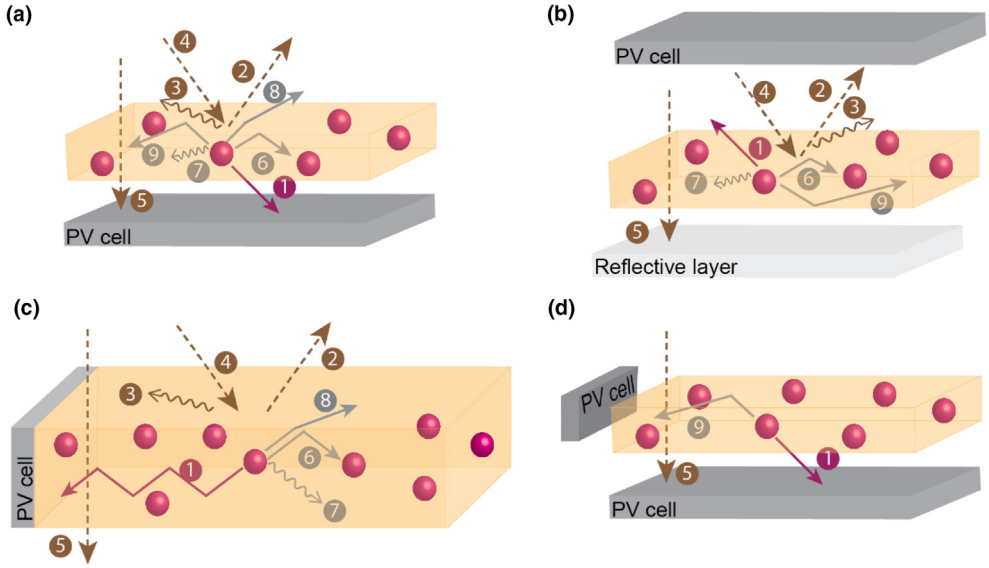

FIGURE 3

Operating principles of spectral conversion devices. Primary processes and losses occurring in (a) DSLs, (b) UCLs and (c) planar LSCs: (1) emission from the optically active center, (2) Fresnel reflections, (3) surface scattering, (4) waveguide attenuation, (5) transmitted radiation, (6) re-absorption by neighbor centers, (7) non-radiative relaxation, (8) emission within the escape cone, (9) radiation lost through the sides, adapted from [13,43]. (d) Schematic representation of a combined device: the LSC harnesses the radiation lost through the DSL lateral sides.

Please cite this article in press as: R.A.S. Ferreira et al., Materials Today, (2019), https://doi.org/10.1016/j.mattod.2019.10.002

subsequently absorbed by the PV cell, producing more electron-hole pairs and thus generating higher short-circuit current (I_{SC}) [13]. This leads to an increase in EQE over the absorption range of the DSL [40]. The open-circuit voltage (V_{OC}) and fill factor (*FF*) should not change significantly upon the incorporation of a DSL since they depend primarily on the intrinsic materials of the PV cell itself [41]. While luminescent DSL could enhance the PV device power conversion efficiency, it is important to note that the design will not be able to overcome the Shockley-Queisser efficiency limit [42].

Recent research has focused on the optimization of host-luminophore combination to improve the stability, efficiency and ease fabrication of the devices. DSLs should be tailored to enhance a specific function of the PV cells in use, and thus, significant research has been dedicated to the design of DSLs for Si PV cells.

As mentioned above, only the absorption of photons with energy higher than the bandgap can generate electron-hole pairs contributing to electric current. The transmission of sub-bandgap photons is one of the major energy loss mechanisms which, for the case of c-Si solar cells, account for losses of about 30% of the incident solar photons [44]. Thus, UC materials may provide a solution to the transmission loss by converting two sub-bandgap photons into one above-bandgap photon (Fig. 3b). The PCE of a solar cell equipped with an upconverter was analyzed through a bifacial single-junction solar cell with an UCL on the rear of the solar panel (Fig. 3b). The maximum PCE was calculated to be 47.6% for non-concentrated light [45].

Although the idea of using UC for improving the performance of PV cell is implicit, one considerable limitation lies in the fact that UC processes are only possible with metastable and long-lived intermediate levels acting as storage reservoirs for the pump energy [16].

In what concerns LSCs that typically consist of a waveguide coated or doped with highly emissive chromophores (Fig. 3c), the sunlight is absorbed by the chromophores and re-emitted at a longer wavelength (or shorter wavelength in case of UC). The emitted radiation propagates to the waveguide edges by total internal reflection, where small PV cells convert it into electricity [46,47].

The optical processes involved in DS/DC/UCLs and LSCs, Fig. 3, are essentially the same and are determinant for the PCE of the devices. The losses associated with the optically active center include non-absorbed photons, low emission QY, re-absorption of emitted photons by neighboring optically active centres. Moreover, in the case of DS/DC/UCLs the guided radiation may be lost through the sides (faces) [17–19]. An innovative strategy may include the harvesting of such guided radiation reaching the edges of the converting layer by additional edge-mounted PV devices, combining in a single PV system DSLs and LSCs (Fig. 3d).

Spectral converters testing

Because of the relatively low technology readiness level of the spectral converters in respect to that of conventional PV, a standardized testing procedure is still missing which often makes very difficult to compare the performances of devices realized by different research groups and companies. These tests are made all the more complicated by the inherent size-dependent efficiency of these devices. Moreover, depending on the take-home message of the different researches, various efficiency meters have been reported, which include the:

i) quantum efficiency, η_Q, i.e., the ratio between the number of collected photons and the number of absorbed ones. This is mainly used to quantify the device ability to suppress the reabsorption/scattering losses.
ii) optical conversion efficiency, η_{opt}, i.e., the ratio between the generated optical power and the incident one. It is used to evaluate the overall optical efficiency of a device disregarding only the optical to electrical conversion efficiency. This parameter tends to penalize the NIR emitters with respect to the visible ones in which the charge carrier thermalization during the optical to electrical conversion reduces the exploitable photon energy.
iii) power conversion efficiency, PCE, i.e., the ratio between the generated electrical power and incident optical one. It is the most relevant parameter for industrial applications even if it does not allow to collect detailed information about the various power loss mechanisms.

The next section reports a summary of the recommended measurement procedures suitable for the evaluation of the different parameters controlling the device performance of an LSC.

Testing procedures

The primary data usually required to characterize a spectral converter, and in particular, an LSC, are the overall efficiency, the capability to suppress the re-absorption and that to avoid any light scattering during the waveguiding process.

For the evaluation of the scattering losses, a simple method has been reported that involves the use of an integrating sphere in which the LSC is placed [48]. Upon excitation, it is necessary to collect the total light output of the LSC and that of the LSC with the edges covered by a tape that absorbs all the waveguided radiation. The comparison between these two measurements gives the fraction of the radiation which escapes from the device surfaces which is expected to be $\left(1-\eta_{trap}\right)$ for a scattering-free slab (η_{trap} is the trapping efficiency). Deviations from the theoretical value are then to be ascribed to the presence of surface/bulk scattering. The limit of this method is that only slabs with a surface area of few tens of cm^2 can be tested in standard integrating spheres. As a consequence, the sensitivity of the method is rather low.

The reabsorption of the emitted radiation due to the overlap between the chromophore absorption and emission spectra can be calculated with propagation tests. They require to excite the LSC with a point source and to measure the spectrum of the radiation escaping from an LSC edge as a function of the excitation distance from the border. This method is very effective because the reabsorption induces relevant changes in the spectrum of the radiation which propagates through the device, thus allowing the evaluation of the losses from relative photoluminescence data [49]. The same method is also suitable for measuring the

Please cite this article in press as: R.A.S. Ferreira et al., Materials Today, (2019), https://doi.org/10.1016/j.mattod.2019.10.002

reabsorption due to the vibrational overtones of the matrix provided that they give rise to well-defined absorption peaks as the main overtones of the C–H stretching vibration modes [50]. However, when several overtones overlap each other to form a uniform background, or if the losses arise from scattering, in the propagation test the spectrum of the collected radiation does not change, and only its intensity decreases by increasing the distance between the excitation-point and the LSC edge. In such a case, the losses must be inferred from absolute intensity measurements which are trickier and require post-processing of the experimental data for compensating the differences into the geometrical collection efficiency for the various positions of the excitation point.

On the basis of the previous discussion, the more reliable and failsafe procedure for evaluating the deviation of an LSC from the ideal behavior is to test if each portion of the LSC surface equally contributes to the total power generated by the device. This can be done by coupling one of the LSC edges with PV cells and reading the power output as a function of the fraction of the illuminated area (piano test) [28,51]. In should be noted that, also for a scattering/reabsorption free device, the contribution to the total collected power of the various LSC slices is not exactly the same because of the different propagation patterns experimented by photons generated in different points, but this effect can be easily calculated or simulated. An example of the expected results of such a test is reported in Fig. 4 that compares the calculated power output *vs*. the illuminated LSC area for some representative conditions. It demonstrates the high sensitivity of the method in the detection of losses due to weak scattering or structureless reabsorption. The last point of this test, in which all the device is illuminated, gives the PCE. From this datum, it is possible to calculate also the η_{opt} and the η_Q provided that the EQE and the current–voltage curve of the PV cells are known.

Because of the utmost relevance for any industrial application of the efficiency measurements, and in particular of the PCE data, here we report a couple of hints useful to avoid obtaining unreliable findings. First of all, it is necessary to test only devices with large area because (i) the LSC performances are size-dependent and (ii) many side effects are only barely detectable in small devices. For lab-scale prototypes, the minimum acceptable linear size should be around 15–20 cm, which should be increased up to 40–50 cm for pre-industrial applications. Second, because these devices are semi-transparent, it could be not negligible the contribution to the overall generated power of the radiation transmitted by the device and then diffused back from the surrounding environment. For this reason, it is important to have absorbing backgrounds, and the test report must indicate how the problem has been addressed. Finally, care should be taken to avoid direct illumination of the PV cell from the excitation source, which can easily happen, especially in outdoor tests.

Light-harvesting and conversion

For spectral converting applications, materials which present tunability of the absorption and emission spectra and large Stokes shift are advantageous. The selection criteria of optically active chromophores for DSLs/DCLs/UCLs are mostly the same as those for LSCs, being the most common ones organic dyes [28–30,43,46,48,52–67], quantum dots (QDs) [41,49,68–85] and lanthanide metal ions/complexes [28,29,42,51,86–101]. In the next sections, selected relevant works will be addressed. We should note that this review only covers examples where device quantification performance was demonstrated.

Light emission key parameters

The active chromophores are the core of any radiation managing system including DSLs, UCLs and LSCs where they are responsible for both absorption and emission phenomena. The ideal chromophore is expected to have a very large QY, as well as a broad and strong absorption for ensuring optimal harvesting of the solar radiation. This second capability can be evaluated through the so-called chromophore spectral coverage, which is the measure of the fraction of absorbed solar power. The spectral coverage is a function of the chromophore concentration and tends to a limit value, which depends only on the absorption edge. It is typically in the range of 30–50% for organic conjugated molecules and organolanthanide complexes, and up to 70% and over for low-bandgap semiconductor QDs. Importantly, the absorption edge does not affect only the achievable spectral coverage but also the color of the devices and, as a consequence, their architectonic integrability [17].

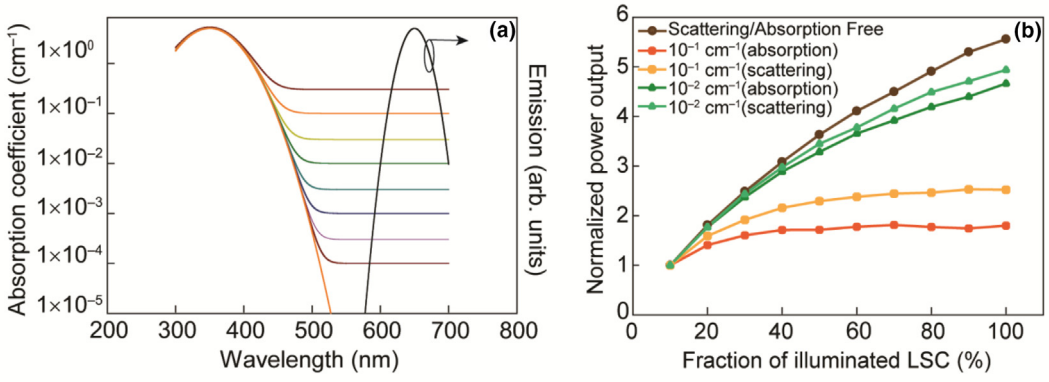

FIGURE 4

Monte-Carlo ray-tracing simulations. (a) Absorption and emission spectra used in the ray-tracing Monte-Carlo simulations. (b) Expected output power vs. fraction of illuminated area for an ideal LSC and for LSCs showing different levels of matrix absorption or scattering.

Please cite this article in press as: R.A.S. Ferreira et al., Materials Today, (2019), https://doi.org/10.1016/j.mattod.2019.10.002

More complex is to define a parameter suitable for quantifying the capability of a chromophore to minimize the reabsorption losses due to the spectral overlap between absorption and emission spectra. This is not so critical for DSLs/DCLs and UCLs, while it is the main factor influencing the performance of large-area LSCs that have been hampering their spread for decades. The Stokes shift between the absorption and emission maxima has been widely used to this aim, but it gives only a rough indication about the reabsorption process because it lacks from any detail nor on the shape of the involved spectra neither on the strength of the absorbing transition. Both modelling and experimental evidence suggest that Stokes shift is not a useful design parameter to identify how well a chromophore performs in a real LSC. For this reason, other parameters have been proposed to quantify the reabsorption process in order to have a reliable tool to compare the performance of different chromophores. An obvious one is the well-known Overlap Integral: $J = \int_0^\infty PL(\lambda)\varepsilon_{Abs}(\lambda)\lambda^4 d\lambda$ [102], where PL and ε are the normalized emission spectrum and the molar extinction coefficient, respectively, as a function of the wavelength (λ). This equation has the advantage to consider the shape of the absorption/emission spectra but can predict wrong performances because it does not consider that large load of chromophores with low absorption coefficient should be necessary to obtain a proper solar radiation harvesting. In order to bypass this problem a variant of the previous equation has been recently suggested [103], which results in a new parameter, unfortunately again named Overlap Integral, $OI = \int_0^\infty PL(\lambda)A(\lambda)d\lambda$, in which the molar extinction coefficient is replaced with the absolute absorption spectrum calculated taking into account transmission (T) and reflection (R), by $A(\lambda) = 1 - T(\lambda) - R(\lambda)$. Therefore, OI is not a property of a specific chromophore but depends also on its amount inside the LSC slab. The point is that it is not possible to define a single optical parameter for a direct comparison of the chromophore capability to reduce the reabsorption losses, because this depends not only on the optical properties of the active species but also on the device size. This can be demonstrated with a ray-tracing simulation routine which enables to calculate the expected power output of an LSC as a function of the optical properties of the active chromophore as well as of the device size. For instance, for LSCs containing two different model chromophores with optical properties depicted in Fig. 5a, the calculated expected performance, considering ideal LSCs (no scattering, no matrix absorption), is shown in Fig. 5b. The first one has been designed to have sharp PL/absorption bands and a small Stokes shift, while in the second the Stokes shift is large, but the optical bands are broad. The absorption spectra have been tailored to ensure the same spectral coverage. It is evident that for small LSC lateral dimensions (around 15–20 cm), the second chromophore outperforms the first one, but the situation is reversed when the LSC size increases. Also keeping constant the LSC area, the chromophore (i. e. keeping constant the Stokes shift and the spectral overlap) and the OI (i. e. keeping constant the light-harvesting efficiency) the performances are not geometry-independent. Indeed, the data in Fig. 5c show that the η_Q increases with the device thickness. This is because the average distance that a photon travels before exiting through the LSC edges is independent of the slab thickness which, on the contrary, determines the density of dispersed chromophores required for an optimal radiation harvesting and, as a consequence, the absorption coefficient in the spectral range of the guided emission.

Even if the findings discussed above show that it is impossible to define a general rule for ranking the chromophores as a function of their capability to mitigate the reabsorption issue, good practices must be followed when comparing LSCs containing different optically active centers: (i) the dimensions of the device must be clearly defined. If large area samples are not available, the expected performances of optically active centers for real-world devices (at least $50 \times 50\ cm^2$) must be extrapolated; (ii) all the comparisons must be made at the same radiation –harvesting level in order not to overestimate the chromophore capability to mitigate the radiation self-absorption only due to its use in low concentration.

QD-based chromophores

Colloidal QDs of many semiconductors can be synthesized by large-scale, low-cost, solution-phase approaches to produce wavelength-tunable chromophores with high QY, narrow spectral feature and high photostability. This has promoted their use as down-shifter of the primary pump emission in the light-emitting diode technology, and today many top-class displays use this approach to extend the color gamut. On the contrary, for decades, QDs were barely employed in LSCs because of the substantial overlap between absorption and emission spectra. The situation has dramatically changed over the last five years, thanks to the discovery of several new strategies for shifting the QD emission far from the corresponding absorption. The first method exploits heterostructured core/shell QD in which a large band-gap shell is grown onto a small band-gap core. If the conduction and valence bands of the core and the shell are properly aligned, all the photogenerated exciton can be promptly localized in the core responsible for the light emission. On the contrary, because the absorption cross-section of a QD is proportional to the number of atoms present in the sample, the core–shell engineering through a thick shell should dominate the absorption properties of the heterostructure. This approach has been applied for the first time in the LSC technology by using core/giant-shell of quasi type-II CdS/CdSe QDs [49] demonstrating, in a 20 cm long poly(methyl methacrylate (PMMA) LSC (Fig. 6a), a reduction of the reabsorption losses of two orders of magnitude in respect to those expected by using core-only QDs. Since the large bandgap of the CdS shell limits its radiation-harvesting capability, other core/shell QDs have been developed for ensuring better harvesting as CdSe/CdPbS QDs [104] and PbS/CdS QDs [68] whose absorption edges extend down to 600 nm and 900 nm, respectively. Importantly, the absorption–emission separation in core/shell QDs can be enlarged by exploiting type-I heterostructures, as $CdSe/Cd_xZn_{1-x}S$, in which a Stokes shift of 0.720 eV has been reported [105].

In giant core–shell heterostructures, the reabsorption is strongly reduced but not completely, because the core absorption is still present. A straightforward evolution of this approach implies that the replacement of the core with the doping of a core-only QD with impurities introduces new localized excited states within the bandgap where the exciton localizes. For

Please cite this article in press as: R.A.S. Ferreira et al., Materials Today, (2019), https://doi.org/10.1016/j.mattod.2019.10.002

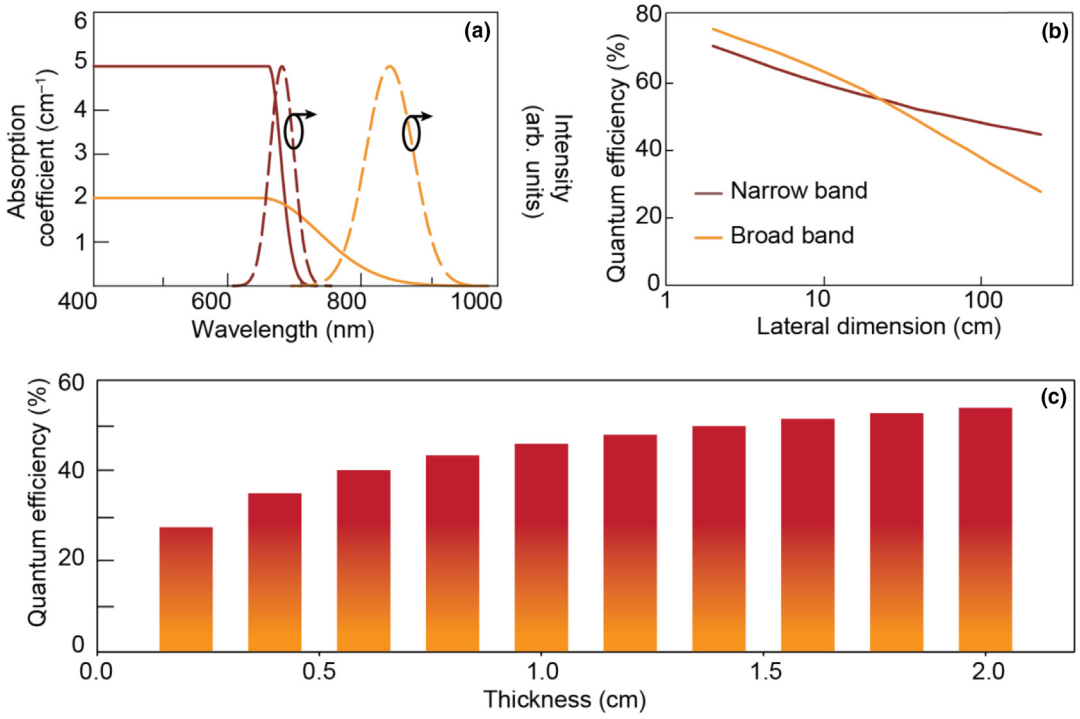

FIGURE 5

Monte-Carlo ray-tracing simulations. (a) Dye absorption (left axis) and emission (right axis) spectra employed in the simulations. The absorption spectra have been scaled in order to harvest the same number of solar photons. (b) The expected quantum efficiency (η_Q) of the LSCs containing dyes with sharp (broad) absorption/emission peaks and a small (large) Stokes-shift as a function of the device lateral dimension. The device thickness is 1 cm, the dye PL QY is 1, and the device is supposed to be free of scattering and matrix absorption. (c) The expected quantum efficiency (η_Q) of the same LSC considered in (b) (broad band) as a function of the device thickness.

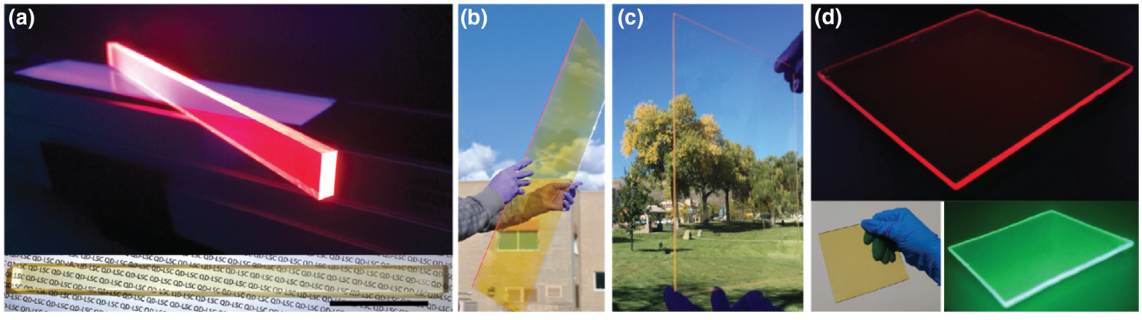

FIGURE 6

Examples of QD-based luminescent solar concentrators. Photographs of large-area LSCs devices comprising (a) CdSe/CdS QDs (21.5 × 1.35 × 0.5 cm^3) illuminated at 365 nm (top) and under ambient illumination (bottom), scale bar, 5 cm. Adapted with permission from Springer Nature DOI: https://doi.org/10.1038/nphoton.2014.54 [49]; (b and c) based on Mn^{2+}-doped QDs under sunlight (b) 91.4 × 30.5 cm^2 and (c) ~413 cm^2, adapted with permission from [105,106], respectively; and (d) Si QDs (12 × 12 × 0.26 cm^3) under ambient (bottom left) and UV illumination at 365 nm) taken with an UV-filtered visible camera (top) and an UV-filtered infrared camera (bottom right), adapted with permission from Springer Nature DOI: https://doi.org/10.1038/nphoton.2017.5 [24]).

instance, Mn^{2+}-doped ZnSe/ZnS QDs have been employed as emitters for reabsorption-free LSCs [75]. Here, the thin shell of ZnS acts only as a surface passivation layer. The Mn^{2+} ions are especially suitable as dopants because they exhibit emission corresponding to a spin forbidden transition with negligible oscillator strength with respect to that of the ZnSe host. Similar results have been obtained by using QDs of $CsPbCl_3$ perovskite as host [107]. However, the absorption of both these hosts, mainly in the UV/blue tail of the solar spectrum, makes the light-harvesting rather inefficient. For this reason, other QD hosts capable of absorbing light down to about 500 nm, such as $Zn_{0.87}Cd_{0.11}$-$Mn_{0.02}Se$/ZnS, have been developed [71]. In view of the emission in the red spectral range, this is probably the best result achievable for an LSC comprising Mn^{2+}-doped QDs. To improve the light-harvesting efficiency of doped QDs, it is necessary to substitute Mn^{2+} ions with other transition metals or rare-earth ions. To this aim, Yb^{3+} is especially promising, not only due to its f–f partially forbidden $^2F_{7/2} \leftrightarrow {}^2F_{5/2}$ transition in the NIR spectral region but also the possibility to feature a QY approaching 200% arising from a quantum-cutting process, similarly to that reported for

Please cite this article in press as: R.A.S. Ferreira et al., Materials Today, (2019), https://doi.org/10.1016/j.mattod.2019.10.002

the Gd^{3+}/Eu^{3+} system verified in powder samples of $LiGdF_4:Eu^{3+}$ in [108]. Recently, a η_Q value of 118% in a 25 cm^2 LSC comprising Yb^{3+}-doped $CsPbCl_3$ perovskite nanocrystals was reported [109]. The only limit of these devices is that the scaling of the LSC size appears to be problematic since the Yb^{3+} emission at ~1000 nm is strongly resonant with the absorption due to the combination of the third overtone of the C–H stretching with the C–H bending vibration. For this reason, salts as CaI_2 and NaCl have been proposed as matrices, when the LSC emission occurs at a wavelength ≥1000 nm [110].

Stokes-shifted emission in QDs can also be obtained without doping but exploiting transitions involving intra-gap states. Following this idea, LSCs based on $CuInS_2$ and $CuInSeS_2$ QDs passivated with a thin ZnS shell have been realized [72]. In such a way, η_{opt} values larger than 3% (device area 144 cm^2) has been demonstrated despite the use of unoptimized QDs. Moreover, the small band-gap of this semiconductor enables the realization of colorless devices, thus facilitating their architectonical integration. These QDs have also been processed into devices using standard doctor-blade deposition obtaining LSCs up to 90 × 30 cm^2 (Fig. 6b) [105], and in tandem architectures which display PCE values as large as 3.1% when coupled to GaAs PV cells (Fig. 6c) [106]. Importantly, in I–III–VI_2 QDs the origin of the states from which the Stokes-shifted emission takes place is still under debate. Originally, it was ascribed to native hole-like defects possibly related to Cu^{2+} ions replacing Cu^{1+} and In^{3+} in adjacent sub-cells or Cu^{2+} paired with a Cu^{1+} [72]. However, first-principle calculations [111], recently supported by experimental evidence [112], suggests that the absorption–emission Stokes-shift is due to a peculiar band structure of these semiconductors which presents a dark-bright splitting of the top of the valence band.

In the rush of realizing much efficient QD-based LSCs, the possibility to suppress the reabsorption losses by exploiting the forbidden transition has not gone unnoticed. In Si-based QDs, the spectral overlap between the absorption of Si and the emission of QDs is minimal due to the QD's indirect bandgap and, thanks to a partial relaxation of the momentum conservation selection rule arising from the quantum confinement, the emission QY can be very high provided that the dots are properly passivated. Moreover, Si-QDs feature a NIR absorption, which accounts for over 50% harvesting of solar radiation. This LSC was demonstrated for the first time in 2017 with η_{opt} values close to 3% in a 12 × 12 cm^2 device (Fig. 6d) [24].

The findings reported above clearly indicate that the QD technology is paving the way for industrial scaling of LSCs, especially considering that many types of LSCs are based on earth-abundant and non-toxic elements.

Lanthanide-based organic complexes

The optical properties of lanthanide-based complexes benefit from the high absorption coefficient of the organic groups and of their ability to efficiently sensitize the long-lived and monochromatic f–f transitions, spanning from the visible to the NIR spectral regions enabling sunlight harvesting and subsequent emission [113]. Additionally, large ligand-induced Stokes shifts are therefore achieved, enabling the design of luminophores with the absorption and emission processes occurring from different energy states. As organic-ligands absorption spectra typically lie on the UV/blue spectral region, the derived lanthanide-based complexes are ideal for use on windows due to their high transparency and colorless nature.

In fact, lanthanides have been proposed as optically active centres for LSCs since very early stages of development. For example, Nd^{3+} was introduced in one of the first published works about LSCs in 1977 [114]. Nevertheless, few works reporting LSCs based on lanthanide optically active centers (Fig. 7a) can be found in the literature [27–29,51,86–90,95,97–100] when compared to LSCs based on organic dyes. For lanthanide-based LSCs, the higher PCE value found was 0.28% for a Si PV cell coupled to an LSC based on PMMA doped with $Eu(tta)_3(TTPO)_2$ (tta = thenoyltrifluoroacetone; TTPO = triphenylphosphine oxide) [99].

Lanthanide-based optically active materials have been more widely used for DSLs (Fig. 7b). Focusing on Si PV cells, theoretical studies state that the maximum PCE gain by applying DSLs to this type of PV cells would be of 0.6–1% [115]. The performance of commercial c-Si and a-Si PV cells is effectively enhanced by surface coating with an organically modified silicate (ORMOSIL) films doped with $[Eu(phen)_2]Cl_3$ (phen = phenanthroline) or $[Tb(bpy)_2]Cl_3$ (bpy = 2,2′-bipyridine), which can convert UV radiation into visible light. The relative PCE values around 118% and 108% for the hybrid c-Si and a-Si PV cells devices, respectively, could be increased by optimizing the incorporation of the lanthanide-based complexes [116]. Several studies used isolated Eu^{3+} or Eu^{2+} ions doped in polymer hosts as DSLs, but the low absorption coefficients associated with lanthanide ions limited the overall efficiency [113,117]. However, the use of Eu^{3+} or Eu^{2+} containing phosphors or complexes has delivered improved performance. Examples include a $Ba_2SiO_4:Eu^{2+}$-based DSL coated directly onto a Si PV cell, in which the addition of Ag nanoparticles and a SiO_2 spacer increased the PCE from 17.1% to 17.7% [118]. A DSL involving $Gd_2O_2S:Eu^{3+}$ phosphors doped in poly (vinylpyrrolidone) with QY = 27–36% was spin-coated onto a mc-Si cell, improving both the antireflection properties and I_{sc}, and increasing the PCE from 10.44% to 12.97% [93]. Besides Eu^{3+} and Eu^{2+} ions, other lanthanide ions have also been investigated for DSLs. For instance, DSLs prepared from $[LnL_3](Et_3NH)_3$ (Ln = Eu,Tb and L = triazole-pyridine-bistetrazolate) dispersed in ethylene vinyl acetate (EVA) deposited by spin-coating yielded an increase in the PCE from 9% to 9.51% and 9.42% for Eu^{3+} and Tb^{3+} analogues, respectively. An $[Eu(tta)_3$-phen] complex was also incorporated in EVA but despite the increase of EQE observed in the UV, the I_{sc} and PCE of the PV cell decrease after deposition of the DSL, probably due to the small loss of EQE observed in the visible part of the spectrum, which can originate from a parasitic absorption in the same region [91].

Other DS phosphors composed of $Y_2O_3:Eu^{3+}$ or $Y_2O_2S:Eu^{3+}$ dispersed in polyvinyl alcohol or PMMA on top of mc-Si PV cell resulted in a fourteen-fold increase in PCE under UV irradiation [120].

Recently, the use of Tb^{3+}- and Eu^{3+}-doped organic–inorganic hybrid materials (di/tri-ureasils) as DSLs layers on c-Si PV cells was reported with an increase of the maximum delivered power and a maximum absolute EQE increase of 14% and 27%, respectively [119], Fig. 7d–f. Also, in this study, a solar-powered car

Please cite this article in press as: R.A.S. Ferreira et al., Materials Today, (2019), https://doi.org/10.1016/j.mattod.2019.10.002

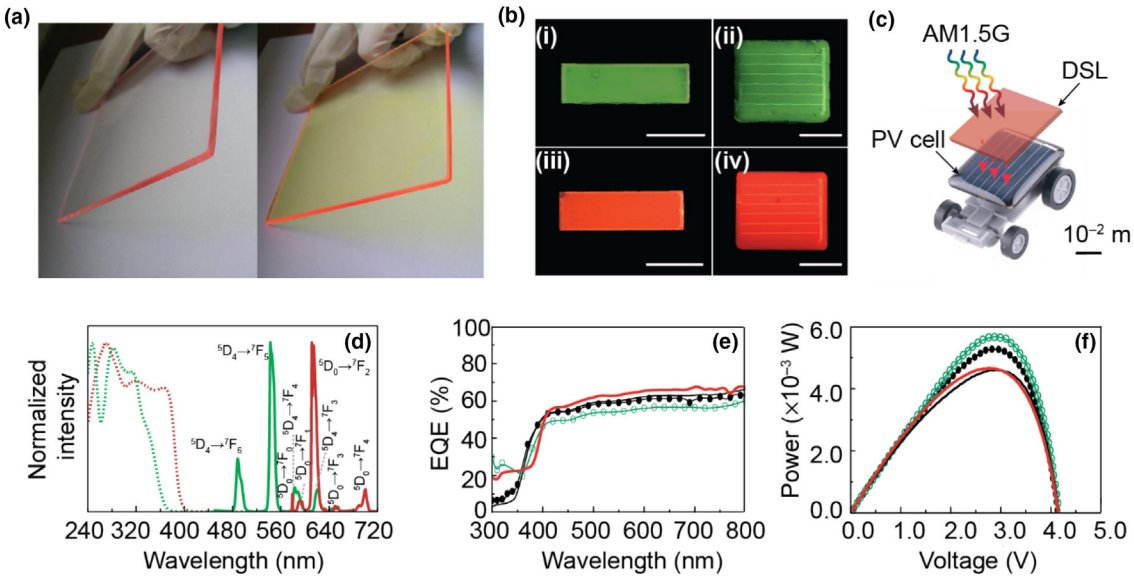

FIGURE 7

Examples of lanthanide-based luminescent solar concentrators and down-shifting layers. Photographs of (a) LSCs based on polyvinyl-butyral doped with Eu(tta)$_3$phen (left) and Eu(tta)$_3$dpbt (right, dpbt = 2-(N,N-diethylanilin-4-yl)-4,6-bis(3,5-dimethylpyr-azol-l-yl)-1,3,5-triazine)) under natural day next to window and (b) c-Si PV cell/panels coated with DSLs based on (i and ii) Tb^{3+} and (iii and iv) Eu^{3+}-doped organic–inorganic hybrid materials, under UV radiation at 365 nm. Scale bars: 10^{-2} m. (c) Scheme of the solar vehicle. (d) Excitation spectra (dashed lines), monitored at 543 nm and 615 nm, for Tb^{3+} (green line) and Eu^{3+} (red line), respectively, and emission spectra (solid lines), excited at 315 nm, for Tb^{3+} (green line), and 365 nm, for Eu^{3+} (red line). (e) EQE and (f) *P* vs *V* curves of the Tb^{3+} (green lines) and Eu^{3+} (red lines) coatings compared with the correspondent bare devices (black lines). Reproduced with permission from [98,119].

(Fig. 6c) race was organized. The small vehicle containing the coated PV cells presented a relative increase of 9% in the velocity when compared to that with the uncoated one [119].

Organic-based dyes

Dye-based coatings are among the most efficient ones with emission QY values approaching 100% and large absorption coefficients, allowing efficient solar radiation harvesting and conversion, thus, have been widely used in PV applications.

Experimental results using c-Si PV cells coated with PMMA doped with DS organic molecules showed an increase of 40% in EQE for wavelengths up to 400 nm [121]. Organic dyes have also been tested as DSLs in other types of PV cells. For instance, Lumogen Violet/Yellow organic dyes were used in CIGS PV cells, yielding to an increase in the EQE from 9% to 52% at 380 nm [55] and, for DSSCs the Lumogen Violet organic dye as DSL lead to over 60% increase in the PV cell PCE values [94]. The same organic dye was tested in perovskite PV cells, which yielded a PCE increase of ~6% [122]. The use of C545T fluorescent molecule doped tris(8-quinolinolate) aluminum in an organic PV cell was also effective by generating a ~15% PCE increase [123]. Another interesting example uses six organic dyes as DSLs for CdTe, CIGS and c-Si PV cells [60], in which, for the case of c-Si PV cells, the authors found that only the Violet 570 dye in EVA rises the device performance (Fig. 8a).

Considering LSC structures (Fig. 8b), the most used organic dyes are the rhodamines [46,114,124,125], coumarins [124–128] and perylene(bisimides) derivatives [67,127–132] due their high emission QY and ε values, despite small Stokes shift and tendency to aggregate via intermolecular π–π stacking interaction between the aromatic rings and the neighboring molecules. Aggregation may lead to either partial or complete quenching due to preferential relaxation via non-radiative channels. The largest η_{opt} value of 18.8% was found for a 5.0 × 5.0 × 0.3 cm^3 LSC based on a plastic plate coated on both sides with yellow and red perylimide dyes, in which the yellow dye-colored surface was facing the incident radiation [125].

Here, we will focus on the potential replacement of synthetic organic dyes by luminescent organic molecules extracted from renewable and natural materials that could make LSCs cheap and sustainable, keeping other inherent features such as synthetic versatility, high absorption coefficients and QY values [133,134].

Natural-based (sustainable) molecules

The most common natural dyes used in LSCs are based on phycobilisomes which are photosynthetic complexes, mainly composed of phycobiliproteins, with light-harvesting ability over a broad range of the visible spectrum [135–137]. Phycobilisomes are promising dyes since donor and acceptor molecules are already aggregated in an ideal configuration [137]. One example is demonstrated in a 22 × 22 × 0.5 mm^3 LSC based on phycobilisomes dispersed in acrylamide films with η_{opt} of 12.5%, quantified through an integrating sphere [136].

R-phycoerythrin (R-PE) is one of the most abundant phycobiliproteins in red macroalgae with high absorption coefficient and emission QY [138]. A recent study on an R-PE based LSC (Fig. 8c) yielded η_{opt} values of ~6.9% and PCE of ~0.27% [30].

Featuring a sustainable route for designing LSCs, photosynthesis may be an inspiring natural mechanism. In this process, one important molecule is chlorophyll as it is responsible for sunlight harvesting [139] with emission properties in the red/

Please cite this article in press as: R.A.S. Ferreira et al., Materials Today, (2019), https://doi.org/10.1016/j.mattod.2019.10.002

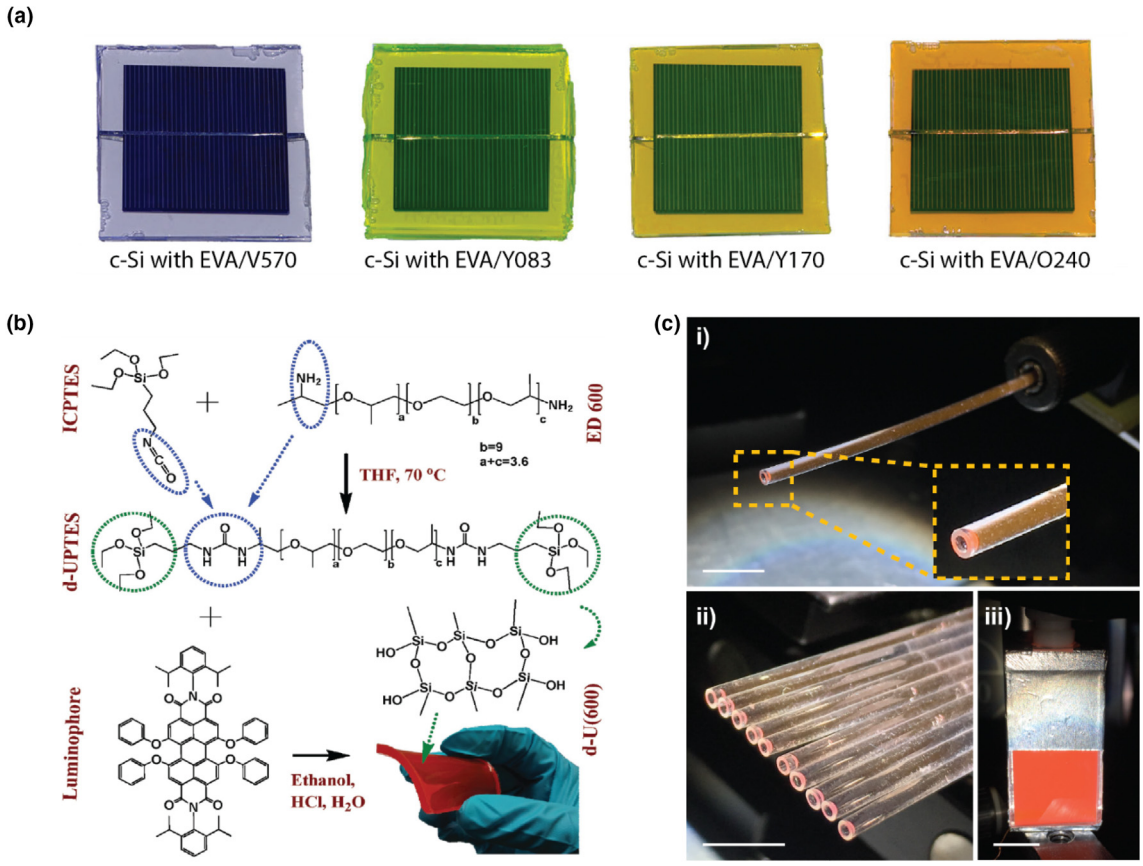

FIGURE 8

Examples of organic dye-based luminescent solar concentrators and down-shifting layers. (a) Selection of c-Si PV cells coated with different DSLs based on EVA doped with Lumogen Violet 570 (V570), Yellow 083 (Y083), Yellow 170 (Y170) and Orange 240 (O240). (b) Schematic representation of the fabrication of a LSC based on an organic–inorganic hybrid doped with an organic dye. A picture of fabricated LSC is shown in the right corner. (c) Photographs of a (i) single and (ii) bundle structure of cylindrical LSCs and (iii) planar LSC based on R-Phycoerythrin aqueous solution under AM1.5G illumination. Scale bars: 10^{-2} m. Reproduced with permission from [60,43,30].

NIR spectral region. Chlorophyll molecules extracted from *Spirulina maxima* were incorporated into organic–inorganic hybrids and characterized as LSCs. These chlorophyll-based LSCs were coupled to a Si-based PV device, revealing η_{opt} and PCE values of $3.70 \pm 0.01\%$ and $0.10 \pm 0.01\%$, respectively, demonstrating the potential of nature-inspired LSCs for sustainable PV energy conversion [52].

UC materials for solar applications

Nearly 50% of the Sun energy in the infrared region is directly wasted due to the incapable absorption of sub-bandgap photons by conventional PV cells. Therefore, an increase in the conversion efficiency could be anticipated if anti-Stokes spectral conversion materials are appropriately introduced to harvest the solar energy in the infrared region (Fig. 1a). There are several UC mechanisms, including excited-state absorption (ESA) or sensitized multiphoton absorption (sMPA), widely exploited in rare-earth-based upconverters. Lanthanide-doped UC nanomaterials hold promise as frequency conversion materials to take on this task since they can absorb infrared photons and subsequently emit photons with wavelengths spanning the spectral region from UV to NIR [140]. Many research groups are focusing on boosting the PCE of Si-based PV cells by incorporating lanthanide-based UC nanomaterials into the devices to convert long-wavelength (>1100 nm) photons to shorter wavelength ones that can be harvested by the solar cells. Despite enormous efforts, the improvement in solar cell PCE is somewhat limited [141–143].

The absorption range of lanthanide ions in the infrared region is very narrow (full-width-at-half-maximum <50 nm), which directly leads to insufficient spectral overlap between radiation absorption of the spectral converters and the solar spectrum [144]. The absorption cross-section of lanthanide ions is also small ($<10^{-19}$ cm^2) as the involved *4f–4f* transition is parity forbidden. [145,146]. Therefore, the overall absorption of infrared solar photons would be quite small even with good spectral overlap, and the UC efficiency is typically low (<1%) upon low power excitation [147], since it is dominated by multiphoton absorptions (Fig. 9a and b).

The coupling of UC nanoparticles with DSSC or perovskite solar cells has shown slight enhancement in overall PCE [148,149]. However, it was further evidenced that the improvement in device performance was attributed to light scattering by small-sized UC nanoparticles, instead of the effect of photon UC. Notably, to validate the contribution of the UC effect toward device improvement, high-power lasers (>10 W·cm^{-2}) are often

Please cite this article in press as: R.A.S. Ferreira et al., Materials Today, (2019), https://doi.org/10.1016/j.mattod.2019.10.002

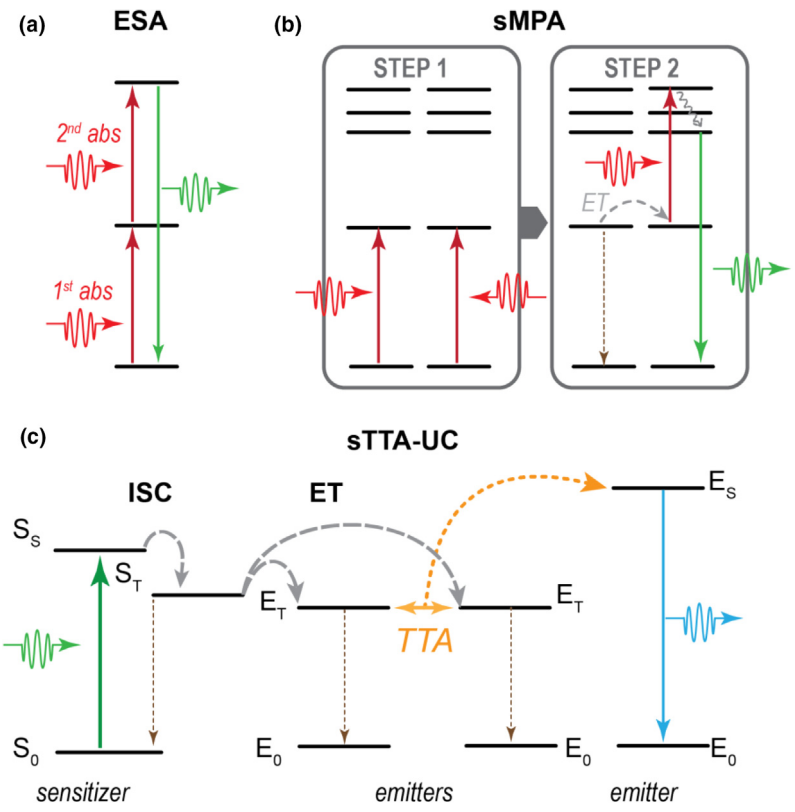

FIGURE 9

Mechanism of upconversion. (a) Excited-state absorption (ESA): the absorption of a first photon allows the transition from the ground state to a first excited state. The sequential absorption of a second photon causes a transition to a higher energy excited state. (b) Sensitized multiphoton absorption (sMPA): after the absorption of two photons by two different chromophores, there is an energy transfer (ET) from one to the other that generates a high-energy excited state that relaxes to an emissive electronic state after a thermalization. (c) Sensitized triplet–triplet annihilation assisted UC (sTTA-UC): the higher energy emissive state (E_S) is generated after triplet–triplet annihilation between emitters (E_T), populated via triplet–triplet ET from a low energy light-harvesting moiety, the sensitizer (S_T). ISC stands for intersystem crossing. Reproduced from Ref. [174] with permission from the PCCP Owner Societies.

used to irradiate the devices containing UC nanomaterials [150]. Lanthanide-doped UC nanomaterials are frequently introduced in the form of nanocomposites for photocatalytic applications [151–155]. While some successful examples have been reported using UC nanomaterials for enhanced catalytic performance under sunlight irradiation, critics might argue that the contribution of the UC effect is minimal.

Unless the intrinsic limitation of lanthanide-doped UC nanomaterials, in terms of weak radiation-harvesting capability and low conversion efficiency, can be solved, it seems unrealistic to use these nanomaterials for solar energy conversion. Nevertheless, it is possible to improve radiation harvesting by coupling the UC nanoparticles with organic dye molecules that act as sensitizers to trap photons with energies across a broad wavelength range. In light of the large absorption cross-section of organic dyes, dye-sensitized UC nanoparticles can enhance absorption while extending the spectral response range in the NIR [156,157]. An even broader wavelength range is further expected by synthetic modification of a plethora of dye molecules. This approach could be a powerful tool for enhancing the UC luminescence of nanoparticles. However, the development of efficient radiation harvesting dyes with high photostability and low spectra interference with UC luminescence remains an open question. Another method for achieving efficient UC emission involves the use of geometrical solar concentrators in the PV cell panel. Straightforward high-power density excitation through focused sunlight can attain a high UC emission intensity but at the expense of overheating. It has been shown that UC efficiency can reach close to 10% at high power excitations [158,159].

Alternative to lanthanide-based systems, the sensitized triplet–triplet annihilation-based UC (sTTA-UC) is a photon UC technique that has been demonstrated with sunlight in 2006 [160–165]. As shown in Fig. 9c, in this UC route the energy absorbed by a sensitizer is transferred to a second moiety, the emitter, by means of a triplet–triplet energy transfer process. Subsequently, two dark emitter triplets undergo triplet–triplet annihilation (TTA) to produce one excited singlet state, from which a photon with high energy is emitted. In optimized solution systems, UC efficiencies >30% have been obtained at excitation power densities comparable to the solar irradiance [166]. Therefore, in the last decade, materials for sTTA-UC are studied intensively to increase their performances further and to cover a large fraction of the solar spectrum [167]. Nowadays, the research on sTTA-UC is focused on the development of solid systems for technological applications. Several examples of prototype sTTA-UC coupled to solar devices already exist. The first integrated amorphous Si/sTTA-UC device has been reported in 2012, demonstrating a clear enhancement of the PV performance of

Please cite this article in press as: R.A.S. Ferreira et al., Materials Today, (2019), https://doi.org/10.1016/j.mattod.2019.10.002

~1% under tens of suns [168]. Later, since most efficient sTTA-UC pairs exploit radiation in the NIR and visible spectral ranges, these materials have been applied to devices with large bandgap, as DSSCs. In 2016, a significant step forward was made by demonstrating an enhancement as high as 13.6% under 1 sun of non-coherent illumination in standard DSSCs combined with sTTA-UC chromophores embedded in flexible polymer films [169]. In parallel, a breakthrough architecture for UC-enhanced dye-sensitized solar cells was proposed [170]. To facilitate the charge separation of the upconverted singlet excitons, an inorganic–organic interface based on self-assembled layers of sTTA-UC molecular pairs on metal oxide surfaces via metal ion linkages was also exploit. Intensity dependence measurements demonstrated that peak UC efficiency could be achieved at sub-solar irradiance, thus leading to the realization of sun power UC-assisted DSSC cell with technologically appealing PCE, which results in ~300 $\mu A \cdot cm^{-2}$ photocurrent production at AM1.5G condition [171]. While these results support the further development of sTTA-UC pairs for NIR-to-visible photon conversion, it is worth pointing out that the sTTA-UC mechanism is especially suited to improve the photocatalytic water splitting (PCWS) performance of cells for hydrogen production, which exploits metal oxides with a near-UV bandgap (~400 nm) as photocatalysts [172]. By recovering the visible spectrum down to 800 nm through sTTA-UC, a huge efficiency increment (>32%) in the hydrogen and photocurrent production is expected, thus further pushing the continuous development of sTTA-UC assisted PCWS devices [173].

Radiation guiding

The ability of a device to guide the radiation has hardly ever been discussed within the community that works in the field of spectral converters despite being a key factor in the operation of the LSCs. This is because the problems associated with the self-absorption of the chromophores overshadowed any other effect. Only recent progress in the development of new emitters has highlighted the importance of the quality of the matrix in which they are dispersed. Neglecting the use of dichroic coatings and mirrors, the amount of radiation trapped in an ideal waveguide can be calculated by using the laws of the geometrical optics. For a planar geometry, the maximum fraction of trapped photons within an ideal waveguide due to total internal reflection is given by $\eta_{trap} = \sqrt{1 - 1/n^2}$, being n the medium refractive index. Similar equations have been derived also for other geometries such as the cylindrical one [175], while for more complex structures the number of trapped photons can be inferred by using Monte Carlo ray-tracing simulation. In any case, for waveguides with n ~1.5, the theoretical η_{trap} is close to 75% that would be adequate for high-efficiency devices. However, this value can be dramatically reduced in the case of non-ideal systems. This has been highlighted in a study in which the influence of the residual absorption of different matrices on the overall efficiency of an LSC based on NIR emitters has been calculated [17].

In order to have a guideline for the matrix selection, Fig. 10 shows how the η_Q of a planar LSC changes as a function of the matrix absorption and of its dimensions. It is evident that only for very small devices, it is possible to tolerate relatively high matrix absorption coefficients such as those of the standard soda-lime glasses which are in the range of 10^{-1} cm^{-1} and above. Already for dimensions around 25 × 25 cm^2 the losses induced by the matrix absorption become severe unless to use materials with high transparency as a high-quality PMMA whose absorption coefficient is between 10^{-3} and 10^{-2} cm^{-1} both in all the visible spectral range and in the NIR down to about 800 nm. For lateral LSC lengths above 1 m, only materials with absorption coefficient below 10^{-3} cm^{-1} would ensure a proper matrix waveguiding. Actually, only perfluorinated polymers, and some optical glasses [176], show absorption coefficients in this range but it is difficult to see how they can be employed for the LSC production because of severe cost and technological constraints.

The same findings are obtained when analyzing the influence on the LSC performances of the matrix scattering instead of its absorption. Indeed, the only difference between these two processes is that, in the case of the absorption, all the absorbed photons are lost, while the scattering simply implies randomization of their propagation direction making the scattering slightly less detrimental than the absorption as demonstrated by the simulations shown in Fig. 10b. It is interesting to note that, since scattering also diffuses the sunlight shining on the panel, for very small device size the scattering should be beneficial. For this reason, several studies carried out on LSC of a few centimeters in size led to think that the scattering could be used to improve the η_{opt} values of these devices. However, the above simulations show that the scattering must be minimized in real-world LSC.

The last factor affecting the waveguiding performance of an LSC is the quality of its surfaces because the photons undergo multiple reflections before reaching the edges. The total internal reflection ensures a 100% reflectivity only for a perfectly smooth interface, but roughness, dust or scratches can easily reduce this value. The extent of this problem depends on the exact geometry of the device and will be more severe for large-area devices. An indication of the effects of the surface scattering can be obtained from the ray-tracing Monte Carlo simulation shown in Fig. 11. Here, we calculated for an ideal device (zero reabsorption and bulk scattering) the distribution of the number of reflections at the LSC surfaces that the photons undergo before being collected. This distribution has then been recalculated for different reflectivity of the interfaces in a 1 m^2 device. A reflectivity of 99% is sufficient to reduce the device performances by 20%, which drop down 50% of the initial value for reflectivity below 95%. In view of the industrialization of these devices, this means that it will be necessary to use only plastic slabs made by casting materials as the extrusion process can hardly guarantee proper roughness. The same applies to thin-film devices.

In conclusion, the influence of the matrix on the waveguiding process must be carefully controlled to realize LSCs suitable for real applications and not only as small lab prototypes.

Optical to electrical conversion

As the waveguiding issue, also the radiation conversion into electrical power is a problem barely investigated so far. Indeed, it is a common practice to report the optical characterization of the devices, completely neglecting the electrical one. When also electrical tests are carried out, the most frequently employed PV cells

Please cite this article in press as: R.A.S. Ferreira et al., Materials Today, (2019), https://doi.org/10.1016/j.mattod.2019.10.002

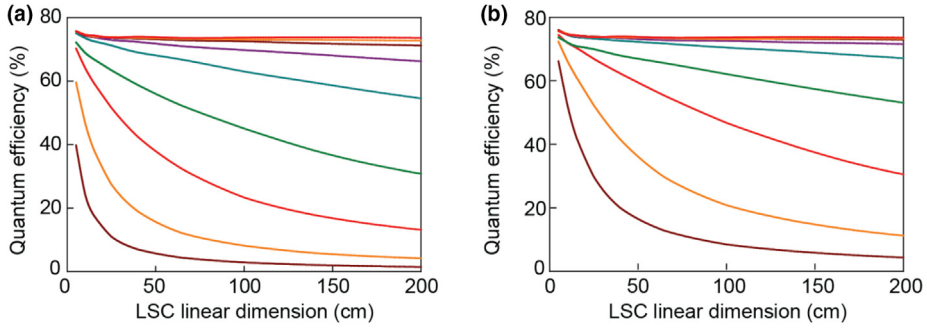

FIGURE 10

Monte-Carlo ray-tracing simulations of the expected efficiency (η_Q) as a function of the device size. The long-wavelength background has been treated as due to (a) matrix absorption or (b) to scattering. Simulation parameter is the same as in Fig. 4.

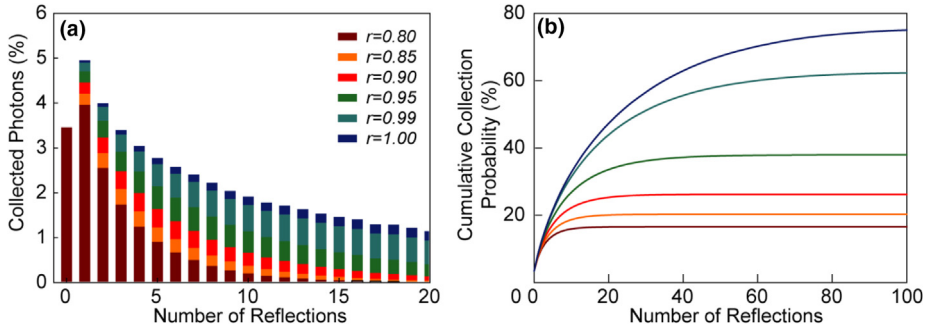

FIGURE 11

Monte-Carlo ray-tracing simulations. (a) Distribution of the reflection numbers experimented by the collected photons in a 1 m^2 ideal LSC (no reabsorption, no bulk scattering) as a function of the interface reflectivity. (b) Cumulative collection probability.

are standard Si cells possibly directly cut from a large wafer to limit their cost [177]. If visible emitters are used for spectral conversion, also GaAs [106,178] and in some cases GaInP [179] PV cells are reported despite both being extremely expensive and not available for the standard market.

The recent advances in the development of more and more efficient LSCs have highlighted the need to reduce the losses due to the electrical conversion step in order to extract properly the largest fraction of the generated optical power. This is a tricky business because the large EQE of most PV cells (for c-Si PV is above 90% from the UV down to 900 nm) ensures to convert nearly all the generated photons into electrons, but it is not the same for their power. In particular, the Shockley–Queisser analysis implies a direct relationship between the semiconductor band-gap and the device V_{oc}, which arises from thermodynamic consideration [180]. For Si PV cells (bandgap ~1.1 eV) the maximum achievable V_{oc}, at room temperature, is slightly above 0.750 V, which decreases to about 0.600 V for commercial PV cells. This means that, even neglecting the impedance matching issue which limits the PV FF below the unit, and even supposing that all the photons collected at the LSC edges are spectrally matched with the PV bandgap (i.e. their energy is 1.1 eV corresponding to a wavelength of 1127 nm) the energy of the generated electrons is only $\frac{0.6}{1.1}$ ~0.5 of the corresponding photon energy. In other words, by using Si PV cells, the optical to electrical conversion implies a PCE loss of at least 50%.

To date, there are still no detailed studies aimed to find the best PV cell to be coupled to an LSC, but many hints can be extracted from simulations [181]. The optical performances of LSCs based on $CuInS_2$/ZnS nanocrystals were calculated and then compared with the expected electrical power generated by coupling different PV cells to the plastic slab edges. Even if some details are dependent on the specific simulated LSC, the general view is clear. For c-Si PV cells, the optical to electrical conversion implies losses around 70% which rise above 90% if a-Si is employed. Slightly better performances are predicted for CdTe PV cells, mainly because of their high V_{oc}, but the sharp absorption edge of this semiconductor at 900 nm prevents its use with dyes with emission extending toward 1000 nm. Environmentally friendly PV cells such as Cu_2ZnSnS_4 have expected performances in between those of c-Si and a-Si. No data have been calculated for GaAs PV cells but, considering its bandgap at 870 nm and a V_{oc}, at room temperature, ~1 V, it is possible to suppose that its PCE should not be much better than that of CdTe.

In the light of the reported results, it is evident that the PCE is becoming the main bottleneck which limits the efficiency of the LSC devices. It is desirable that the rapidly growing interest for this technology will stimulate the leading PV manufacturers to design new production lines of PV devices tailored to have their best performances when used with nearly monochromatic NIR emissions and not when illuminated with white light.

Please cite this article in press as: R.A.S. Ferreira et al., Materials Today, (2019), https://doi.org/10.1016/j.mattod.2019.10.002

LSC devices: the role of the geometry

Planar vs. cylindrical LSC

The planar LSC configuration enables PV devices to be embedded in building façades or windows, contributing to the development of zero energy buildings [18], and other architectonic elements [33–35]. The interest in fabricating transparent LSC windows has been on the rise using NIR-emitting or UV-absorbing optically active centers [182]. The LSCs showed promising results, towards the use of these novel materials as transparent PV windows for urban integration of light-harvesting devices [24,49,72,86,96,183]. Moreover, the use of planar LSCs as windows may also have applicability for "smart" windows, in which the transmitted spectra, haze, and intensity can be directly regulated by applying a voltage and simultaneously generate electrical power, as both functions could be incorporated in one single module [184].

Nevertheless, the choice of LSC geometry may influence the device overall performance. Theoretical works suggest that cylindrical geometry allows an increase of the concentration factor ($F = G \times \eta_{opt}$, in which G is the geometrical gain given by the ratio between the surface and edge areas of the LSC) [26,29,80,185,186] which can be very large for optical fiber-shaped LSC. When diffuse radiation is considered instead of direct one, the high G value of cylindrical LSCs has great advantages when used under cloudy weather conditions, at shaded locations and in situations where direct irradiance is scarce or absent [26].

Also, theoretical studies suggest that the assembling of cylindrical LSCs in a multi-cylindrical bundle structure may induce an additional increase in the optical concentration of at least ~4.5%, relative to single cylindrical LSCs. Cylindrical LSCs take advantage of multiple reflections between neighboring cylinders and fewer surface reflections for any angle of incidence [186,187], which may result in a ~2-fold increase in the optical concentration as compared to planar LSCs. These results were experimentally tested by constructing a multi-cylindrical bundle and a layered planar LSC based on PMMA slabs with the same surface area of the bundle [29], resulting in lower η_{opt} values measured for the planar LSC (1.54 ± 0.01%), relatively to that found for the bundle structure (5.28 ± 0.01%), revealing an increase of 3.5 times in the η_{opt} values [29].

Optical fiber LSCs

Vitreous and polymer fibers are produced on large scales with optimized and low manufacturing costs and, thus, can be used to fabricate cylindrical LSCs [26,80,185,186], promoting new research ideas in interdisciplinary and emerging fields [27–29,51,58,80,188]. The intrinsic properties of the fibers themselves also present advantages for LSC applications: lightweight, flexibility and possibility of coupling to other optical fibers for waveguiding [30]. These attributes allow remote radiation-harvesting and the creation of new applications, such as light optimization in greenhouses [37], mobile applications and indoor daylighting.

Moreover, considering the larger G factor of fibers compared to planar geometry, increasing the surface area of cylindrical LSCs is an interesting strategy, despite the effective propagation length should be taken into consideration if larger absorption coefficients (above 10^{-3} cm^{-1}) characterize the waveguide medium, as noticed above for planar LSCs.

Two strategies were implemented by fabricating LSCs based on (i) bundle-assembled fibers and (ii) long-length (meter scale) optical fibers. Besides theoretical studies, experimental fiber bundle structures were first proposed in 2013 [189]. Recently, a study reporting bundle structures of triangular hollow-core POFs filled with organic–inorganic hybrid materials doped with Rhodamine 6G, Rhodamine 800, or a Eu^{3+} β-diketonate complex was published [29]. In this case, the assembling is favored by the fiber's triangular cross-section that also maximizes the coverage of a PV cell surface. Bundles incorporating each material were constructed, as well as one bundle combining all the materials, yielding a maximum PCE value of 0.74%.

The use of sustainable optically active centres was also tested in a fiber bundle configuration by which the hollow-core POFs,

FIGURE 12

Meter-scale cylindrical luminescent solar concentrators. Long-length fiber LSCs based on bulk-coated and hollow-core POFs in which the optically active layer was based on organic–inorganic hybrids doped with a Eu^{3+}-based complex and Rhodamine 6G. Adapted with permission from [28].

Please cite this article in press as: R.A.S. Ferreira et al., Materials Today, (2019), https://doi.org/10.1016/j.mattod.2019.10.002

filled with R-PE aqueous solutions and assembled side-by-side, could yield η_{opt} and PCE values of ~4.74% and ~23.03×10^{-3}%, respectively [30].

The use of long-length fibers in an LSC was first reported in 2010, based on a PMMA plate with 150 pieces of 1 m long fibers with three colors. This device, mounted on a roof, could transport the concentrated light to a remote dark room, clearly showing a pleasant potential in remote indoor daylighting. In 2016, meter-scale fiber LSCs based on bulk-coated and hollow-core plastic optical fibers (POFs) were also reported [28]. In this work, the optically active materials were based on organic–inorganic hybrids doped with a Eu^{3+} complex or Rhodamine 6G (Fig. 12). The hollow-core-optimized device displayed $\eta_{opt} = 8.0\%$, a value among the highest reported so far.

More recently, PMMA-based fibers doped with a combination of organic dyes and metal–organic materials were fabricated by employing bulk polymerization and a fiber drawing process. Active fiber lengths of more than 6 m were reported, with output intensities of ~1.3 $mW \cdot mm^{-2}$ and photostability studies revealing a level of performance equal to 64% of the initial value after 600 h of continuous solar exposure [190].

Conclusions and future directions

This review presented the fundamentals and an overview of existing technologies and materials for the improvement of photovoltaic (PV) energy production through spectral conversion. The main goals for the application of such converters are to increase the architectonic integration of the PV systems and to improve their performances by enhancing the match between the solar spectrum and the PV cells absorption.

Upconversion is an optical process in which sub-bandgap sunlight is harvested and converted to higher energy photons. A promising approach lies on low-power sensitized triplet–triplet annihilation-based upconversion in organic molecules for wide bandgap solar cells since it allows efficient NIR-to-visible conversion. In down-conversion, high-energy above-bandgap photons are absorbed, in a process that can yield an emission quantum yield of 200% and improve the generate-electron/incident-photon ratio of narrow bandgap solar cells such as crystalline-Si solar cells. The application of down-shifting materials is likely to improve the spectral response of solar cells to short-wavelength photons in a one-to-one photon conversion process.

Spectral converters may be deposited as layers directly on the surface of the PV cell to convert the incident sunlight or as luminescent solar concentrators to concentrate radiation and subsequently direct the concentrated radiation into a relatively small output target. The LSC technology has gained considerable visibility since it can integrate PV devices into buildings in the form of colorless solar windows and contribute to the achievement of zero energy buildings.

In the future, researchers working on spectral conversion materials and devices should engage their efforts on the optimization of the efficiency of real-world size devices (meter scale) and, inevitably, work on the optimization of the optical features of both the optically active centers and the host matrix/waveguides in order to minimize associated losses.

The interest in PV complementary spectral converters is a growing issue due to their stated potential in enhancing the use of solar energy for a better and more sustainable future.

Acknowledgments

This work was supported by the projects CICECO-Aveiro Institute of Materials, POCI-01-0145-FEDER-007679 (FCT Ref. UID/CTM/50011/2019), SusPhotoSolutions – Soluções Fotovoltaicas Sustentáveis, CENTRO-01-0145-FEDER-000005, SolarFlex, CENTRO-01-0145-FEDER-030186, financed by national funds through the FCT/MEC and when appropriate co-financed by FEDER under the PT2020 Partnership Agreement. FM acknowledges the financial support from the Italian Ministry of University and Research (MIUR) through grant "Dipartimenti di Eccellenza-2017 "Materials For Energy".

References

[1] Transforming our world: the 2030 Agenda for Sustainable Development. https://sustainabledevelopment.un.org/, 2019 (accessed May 2, 2019).
[2] Abergel, T., et al., 2018 Global Status Report: Towards a zero-emission efficient and resilient buildings and construction sector, International Energy Agency, 2018, (accessed October 20, 2019).
[3] P. Torcellini et al., A Common Definition for Zero Energy Buildings, The National Institute of Building Sciences, 2015. https://www.energy.gov/ (accessed October 20, 2019).
[4] P. Torcellini et al., Zero Energy Buildings: A Critical Look at the Definition, National Renewable Energy Laboratory, 2006. https://www.nrel.gov/docs/fy06osti/39833.pdf (accessed October 20, 2019).
[5] C. Philibert, Solar Energy Perspectives, International Energy Agency, OECD/IEA, 2011 (accessed October 20, 2019).
[6] M.A. Green et al., Prog. Photovolt. Res. Appl. 27 (2019) 565.
[7] R. Harikisun, H. Desilvestro, Sol. Energy 85 (2011) 1179.
[8] S.F.H. Correia et al., J. Mater. Chem. A 2 (2014) 5580.
[9] G. Hodes, Science 342 (2013) 317.
[10] Photovoltaics Report, Fraunhofer Institute for Solar Energy Systems, ISE with support of PSE Conferences & Consulting GmbH, Freiburg, 14 March 2019, https://www.ise.fraunhofer.de/content/dam/ise/de/documents/publications/studies/Photovoltaics-Report.pdf (accessed September 17, 2019).
[11] A.M. Hermann, Sol. Energy 29 (1982) 323.
[12] D. Li, G. Chen, Upconversion-enhanced dye-sensitized solar cells, in: M. Soroush, K.K.S. Lau (Eds.), Dye-Sensitized Solar Cells: Mathematical Modeling, and Materials Design and Optimization, Elsevier Inc., Academic Press, 2019, pp. 325–340.
[13] E. Klampaftis et al., Sol. Energy Mater. Sol. Cells 93 (2009) 1182.
[14] B.M. van der Ende et al., Phys. Chem. Chem. Phys. 11 (2009) 11081.
[15] J.-C.G. Bünzli, A.-S. Chauvin, Lanthanides in solar energy conversion, in: J.-C.G. Bünzli, V.K. Pecharsky (Eds.), Handbook on the Physics and Chemistry of Rare-Earths, Elsevier B. V, Amsterdam, 2014, pp. 169–282.
[16] X. Huang et al., Chem. Soc. Rev. 42 (2013) 173.
[17] F. Meinardi et al., Nat. Rev. Mater. 2 (2017) 17072.
[18] B. McKenna, R.C. Evans, Adv. Mater. 29 (2017) 1606491.
[19] M.G. Debije, P.P.C. Verbunt, Adv. Energy Mater. 2 (2012) 12.
[20] F. Purcell-Milton, Y.K. Gun'ko, J. Mater. Chem. 22 (2012) 16687.
[21] R. Reisfeld, Opt. Mater. 32 (2010) 850.
[22] W.G.J.H.M. van Sark et al., Opt. Express 16 (2008) 21773.
[23] B.S. Richards, Sol. Energy Mater. Sol. Cells 90 (2006) 2329.
[24] F. Meinardi et al., Nat. Photonics 11 (2017) 177.
[25] F.M. Vossen et al., Energy Build. 113 (2016) 123.
[26] G. Colantuono et al., J. Lightwave Technol. 31 (2013) 1033.
[27] S.F.H. Correia et al., Sol. Energy Mater. Sol. Cells 138 (2015) 51.
[28] S.F.H. Correia et al., Prog. Photovoltaics Res. Appl. 24 (2016) 1178.
[29] S.F.H. Correia et al., Adv. Sustainable Syst. 2 (2018) 1800002.
[30] A.R. Frias et al., Adv. Sustainable Syst. 3 (2019) 1800134.
[31] Y. Li et al., J. Polym. Sci. A 57 (2018) 201.
[32] M.G. Debije, V.A. Rajkumar, Sol. Energy 122 (2015) 334.
[33] M. Kanellis et al., Renew. Energ. 103 (2017) 647.
[34] M.G. Debije et al., Renew. Energ. 113 (2017) 1288.
[35] M.G. Debije et al., Renew. Energ. 116 (2018) 335.

Please cite this article in press as: R.A.S. Ferreira et al., Materials Today, (2019), https://doi.org/10.1016/j.mattod.2019.10.002

[36] Glass to Power. https://www.glasstopower.com/g2p/, (accessed June 24, 2019).
[37] UbiQD – Ubiquitous Quantum Dots. https://ubiqd.com/, (accessed June 24, 2019).
[38] P.M. Pattison et al., Nature 563 (2018) 493.
[39] UbiGro – Spectrum-controlled greenhouses. https://ubigro.com/, (accessed July 5, 2017).
[40] G.J.J. Draaisma et al., J. Mater. Chem. C 4 (2016) 5747.
[41] S.D. Hodgson et al., Nano Energy 4 (2014) 1.
[42] D.K. Boer et al., Opt. Express 20 (2012) A395.
[43] A. Kaniyoor et al., Adv. Opt. Mater. 4 (2015) 444.
[44] Y.F. Shang et al., Nanomaterials 5 (2015) 1782.
[45] T. Trupke et al., J. Appl. Phys. 92 (2002).
[46] W.H. Weber, J. Lambe, Appl. Opt. 15 (1976) 2299.
[47] R. Reisfeld, S. Neuman, Nature 274 (1978) 144.
[48] M.J. Currie et al., Science 321 (2008) 226.
[49] F. Meinardi et al., Nat. Photonics 8 (2014) 392.
[50] J.P. Harmon, Polymers for optical fibers and waveguides: an overview, in: Optical Polymers, American Chemical Society, ACS Symposium Series23, 2001, p. 1.
[51] W. Wu et al., Sol. Energy 84 (2010) 2140.
[52] A.R. Frias et al., J. Mater. Chem. A 6 (2018) 8712.
[53] R. Rondão et al., ACS Appl. Mater. Interfaces 9 (2017) 12540.
[54] C. Tummeltshammer et al., Opt. Lett. 41 (2016) 713.
[55] A. Solodovnyk et al., Energy. Technol. 4 (2016) 385.
[56] W. Zhou et al., Sol. Energy 120 (2015) 419.
[57] Y. Zhang et al., Energy Convers. Manage. 95 (2015) 187.
[58] E.-H. Banaei, A.F. Abouraddy, Prog. Photovoltaics Res. Appl. 23 (2015) 403.
[59] C. Liu, B. Li, J. Optics 17 (2015) 025901.
[60] D. Alonso-Alvarez et al., Prog. Photovoltaics 23 (2015) 479.
[61] T.S. Parel et al., Sol. Energy Mater. Sol. Cells 140 (2015) 306.
[62] S.F. Daorta et al., Appl. Phys. Lett. 104 (2014) 153901.
[63] Y.M. Zhao et al., Adv. Opt. Mater. 2 (2014) 606.
[64] S.M. El-Bashir et al., Renewable Energy 63 (2014) 642.
[65] P.T.M. Albers et al., Sol. Energy 95 (2013) 216.
[66] G. Maggioni et al., Sol. Energy Mater. Sol. Cells 108 (2013) 27.
[67] A.F. Mansour, Polym. Test. 17 (1998) 153.
[68] Y. Zhou et al., Adv. Energy Mater. 6 (2016) 1501913.
[69] Y.H. Ghymn et al., Nanoscale 7 (2015) 18642.
[70] M. Hong et al., RSC Adv. 5 (2015) 102682.
[71] L.R. Bradshaw et al., Nano Lett. 15 (2015) 1315.
[72] F. Meinardi et al., Nat. Nanotechnol. 10 (2015) 878.
[73] K.E. Knowles et al., Chem. Commun. 51 (2015) 9129.
[74] I. Coropceanu, M.G. Bawendi, Nano Lett. 14 (2014) 4097.
[75] C.S. Erickson et al., ACS Nano 8 (2014) 3461.
[76] Y.L. Li et al., Phys. Chem. Chem. Phys. 16 (2014) 26193.
[77] Z. Krumer et al., Sol. Energy Mater. Sol. Cells 111 (2013) 57.
[78] U. Aeberhard et al., Phys. Chem. Chem. Phys. 14 (2012) 16223.
[79] J. Bomm et al., Sol. Energy Mater. Sol. Cells 95 (2011) 2087.
[80] R.H. Inman et al., Opt. Express 19 (2011) 24308.
[81] G.V. Shcherbatyuk et al., Appl. Phys. Lett. 96 (2010) 191901.
[82] M.G. Hyldahl et al., Sol. Energy 83 (2009) 566.
[83] P.P.C. Verbunt et al., Adv. Funct. Mater. 19 (2009) 2714.
[84] M. Kennedy et al., Sol. Energy 83 (2009) 978.
[85] V. Sholin et al., J. Appl. Phys. 101 (2007) 123114.
[86] A.R. Frias et al., Energies 12 (2019) 451.
[87] V.T. Freitas et al., ACS Appl. Mater. Interfaces 7 (2015) 8770.
[88] J. Graffion et al., J. Mater. Chem. 22 (2012).
[89] J. Graffion et al., Chem. Mater. 23 (2011) 4773.
[90] M. Tonezzer et al., Prog. Photovoltaics Res. Appl. 23 (2015) 1037.
[91] T. Fix et al., Prog. Photovoltaics Res. Appl. 24 (2016) 1251.
[92] M.M. Nolasco et al., J. Mater. Chem. A 1 (2013) 7339.
[93] W.B. Hung, T.M. Chen, Sol. Energy Mater. Sol. Cells 133 (2015) 39.
[94] E. Cattaruzza et al., Sol. Energy Mater. Sol. Cells 130 (2014) 272.
[95] C. Liu et al., Int. J. Photoenergy 2014 (2014) 290952.
[96] A. Sanguineti et al., Phys. Chem. Chem. Phys. 14 (2012) 6452.
[97] I.S. Grigoryev et al., Nanotechnol. Russ. 7 (2012) 492.
[98] X. Wang et al., Sol. Energy 85 (2011) 2179.
[99] T.X. Wang et al., Sol. Energy 85 (2011) 2571.
[100] B. Jezowskatrzebiatowska et al., Sol. Energy Mater. 13 (1986) 267.
[101] K. Kawano et al., Sol. Energy Mater. Sol. Cells 48 (1997) 35.
[102] R. Mazzaro, A. Vomiero, Adv. Energy Mater. 8 (2018) 1801903.
[103] C.C. Yang et al., Sci. Rep. 8 (2018) 16359.
[104] H.G. Zhao et al., Small 12 (2016) 5354.
[105] H.B. Li et al., Nat. Energy 1 (2016) 16157.
[106] K.F. Wu et al., Nat. Photonics 12 (2018) 105.
[107] F. Meinardi et al., ACS Energy Lett. 2 (2017) 2368.
[108] R.T. Wegh et al., Science 283 (1999) 663.
[109] X. Luo et al., Nano Lett. 19 (2019) 338.
[110] O.M. ten Kate et al., Sol. Energy Mater. Sol. Cells 140 (2015) 115.
[111] A. Shabaev, Phys. Rev. B 92 (2015) 035431.
[112] Meinardi, F., in press (2019).
[113] L.D. Carlos et al., Adv. Mater. 21 (2009) 509.
[114] J.A. Levitt, W.H. Weber, Appl. Optics 16 (1977) 2684.
[115] C.P. Thomas et al., Sol. Energy Mater. Sol. Cells 98 (2012) 455.
[116] T. Jin et al., J. Electrochem. Soc. 144 (1997) 4054.
[117] C. Strümpel et al., Sol. Energy Mater. Sol. Cells 91 (2007) 238.
[118] J.Y. Chen et al., Sol. Energy Mater. Sol. Cells 120 (2014) 168.
[119] S.F.H. Correia et al., Opto-Electron. Adv. 2 (2019) 190006.
[120] P. Chung et al., J. Vac. Sci. Technol., A 25 (2007).
[121] K.R. McIntosh et al., Prog. Photovoltaics Res. Appl. 17 (2009) 191.
[122] F. Bella et al., Science 354 (2016) 203.
[123] G.F. Ma et al., Appl. Phys. Lett. 103 (2013) 043302.
[124] B.A. Swartz et al., Opt. Lett. 1 (1977) 73.
[125] J.M. Drake et al., Appl. Optics 21 (1982) 2945.
[126] J.S. Batchelder et al., Appl. Optics 20 (1981) 3733.
[127] A.F. Mansour et al., Polym. Test. 24 (2005) 519.
[128] R. Kinderman et al., J. Sol. Energy Trans. ASME 129 (2007) 277.
[129] R. Reisfeld et al., Sol. Energy Mater. Sol. Cells 33 (1994) 417.
[130] M.G. Debije et al., Appl. Optics 47 (2008) 6763.
[131] M.G. Debije et al., Appl. Optics 50 (2011) 163.
[132] R. Reisfeld et al., Sol. Energy Mater. 17 (1988) 439.
[133] N.J.L.K. Davis et al., J. Mater. Chem. C 5 (2017) 1952.
[134] A. Dey et al., Mater. Today Proc. 3 (2016) 3498.
[135] A.N. Glazer, Methods Enzymol. 167 (1988) 291.
[136] C.L. Mulder et al., Adv. Mater. 21 (2009) 3181.
[137] R. Bose et al., Resonance energy transfer in luminescent solar concentrators, 35th IEEE Photovoltaic Specialists Conference, Honolulu, USA, 2010.
[138] M. Martins et al., Green Chem. 18 (2016) 4287.
[139] B. Demmig-Adams, W.W. Adams, Nature 403 (2000) 391.
[140] G.Y. Chen et al., Acc. Chem. Res. 46 (2013) 1474.
[141] L.L. Liang et al., Chem. Commun. 49 (2013) 3958.
[142] J. de Wild et al., Sol. Energy Mater. Sol. Cells 94 (2010) 2395.
[143] J. de Wild et al., Sol. Energy Mater. Sol. Cells 94 (2010) 1919.
[144] F.Z. Chen et al., Sci. Rep. 5 (2015) 10676.
[145] A. Albalawi et al., Opt. Quantum Electron. 48 (2016).
[146] X.J. Xie et al., J. Am. Chem. Soc. 135 (2013) 12608.
[147] J.C. Boyer, F.C.J.M. van Veggel, Nanoscale 2 (2010) 1417.
[148] L.L. Liang et al., Adv. Mater. 25 (2013) 2174.
[149] L. Liang et al., Nano Lett. 19 (2019) 1796.
[150] M. He et al., Angew. Chem. Int. Ed. 55 (2016) 4280.
[151] R. Adhikari et al., J. Solid State Chem. 209 (2014) 74.
[152] L. Ren et al., J. Mater. Chem. 22 (2012) 11765.
[153] J. Wang et al., Appl. Catal. A: Gen. 334 (2008) 227.
[154] W. Wang et al., Appl. Catal. B: Environ. 144 (2014) 379.
[155] W.F. Yang et al., Nanotechnology 25 (2014) 482001.
[156] W.Q. Zou et al., Nat. Photonics 6 (2012) 560.
[157] G.Y. Chen et al., Nano Lett. 15 (2015) 7400.
[158] S. Fischer et al., Sol. Energy Mater. Sol. Cells 136 (2015) 127.
[159] S. Fischer et al., J. Lumin. 153 (2014) 281.
[160] S. Baluschev et al., Phys. Rev. Lett. 97 (2006) 143903.
[161] T.N. Singh-Rachford, F.N. Castellano, Coord. Chem. Rev. 254 (2010) 2560.
[162] J.Z. Zhao et al., RSC Adv. 1 (2011) 937.
[163] J. Zhou et al., Chem. Rev. 115 (2015).
[164] T.F. Schulze, T.W. Schmidt, Energy Environ. Sci. 8 (2015) 103.
[165] M.K. Manna et al., Chem. Commun. 54 (2018).
[166] S. Hoseinkhani et al., Phys. Chem. Chem. Phys. 17 (2015) 4020.
[167] Y.V. Aulin et al., RSC Adv. 5 (2015) 107896.
[168] T.F. Schulze et al., J. Phys. Chem. C 116 (2012) 22794.
[169] C.H. Li et al., ACS Photonics 3 (2016) 784.
[170] S.P. Hill et al., J. Phys. Chem. Lett. 6 (2015).
[171] Y. Zhou et al., ACS Energy Lett. 4 (2019) 1458.
[172] A. Monguzzi et al., ACS Appl. Mater. Interfaces 9 (2017) 40180.
[173] H.I. Kim et al., Energy Environ. Sci. 9 (2016) 1063.
[174] J. Pedrini et al., Phys. Chem. Chem. Phys. 20 (2018) 9745.
[175] J.D. Weiss, Opt. Eng. 54 (2015) 027101.
[176] A.R. Blythe, J.R. Vinson, Polym. Adv. Technol. 11 (2000) 601.

Please cite this article in press as: R.A.S. Ferreira et al., Materials Today, (2019), https://doi.org/10.1016/j.mattod.2019.10.002

[177] W. van Sark et al., Solar RRL 1 (2017) 1600015.
[178] L.H. Slooff et al., Phys. Status Solidi RRL 2 (2008) 257.
[179] J.C. Goldschmidt et al., Sol. Energy Mater. Sol. Cells 93 (2009) 176.
[180] P. Baruch et al., Sol. Energy Mater. Sol. Cells 36 (1995) 201.
[181] R. Lesyuk et al., J. Mater. Chem. C 5 (2017) 11790.
[182] P. Moraitis et al., Opt. Mater. 84 (2018) 636.
[183] Y.M. Zhao, R.R. Lunt, Adv. Energy Mater. 3 (2013) 1143.
[184] J.A.H.P. Sol et al., Adv. Energy Mater. 8 (2018) 1702922.
[185] O.Y. Edelenbosch et al., Opt. Express 21 (2013) A503.
[186] K.R. McIntosh et al., Appl. Phys. B 88 (2007) 285.
[187] J.J.H. Videira et al., Cylindrical and square fibre luminescent solar concentrators: experimental and simulation comparisons, 40th IEEE Photovoltaic Specialist Conference, Denver, USA, 2014.
[188] C. Wang et al., J. Energy Eng. 136 (2010) 76.
[189] E.H. Banaei, A.F. Abouraddy (Eds.), Proc. SPIE 8821, High and Low Concentrator Systems for Solar Electric Applications VIII, 2013.
[190] I. Parola et al., Sol. Energy Mater. Sol. Cells 178 (2018) 20.

Please cite this article in press as: R.A.S. Ferreira et al., Materials Today, (2019), https://doi.org/10.1016/j.mattod.2019.10.002